

# ENHANCEMENT OF A SUNSPOT LIGHT WALL WITH EXTERNAL DISTURBANCES

SHUHONG YANG<sup>1,2</sup>, JUN ZHANG<sup>1,2</sup>, AND ROBERT ERDÉLYI<sup>3</sup>

*Accepted for publication in ApJL*

## ABSTRACT

Based on the *Interface Region Imaging Spectrograph* observations, we study the response of a solar sunspot light wall to external disturbances. A flare occurrence near the light wall caused material to erupt from the lower solar atmosphere into the corona. Some material falls back to the solar surface, and hits the light bridge (i.e., the base of the light wall), then sudden brightenings appear at the wall base followed by the rise of wall top, leading to an increase of the wall height. Once the brightness of the wall base fades, the height of the light wall begins to decrease. Five hours later, another nearby flare takes place, a bright channel is formed that extends from the flare towards the light bridge. Although no obvious material flow along the bright channel is found, some ejected material is conjectured to reach the light bridge. Subsequently, the wall base brightens and the wall height begins to increase again. Once more, when the brightness of the wall base decays, the wall top fluctuates to lower heights. We suggest, based on the observed cases, that the interaction of falling material and ejected flare material with the light wall results in the brightenings of wall base and causes the height of the light wall to increase. Our results reveal that the light wall can be not only powered by the linkage of  $p$ -mode from below the photosphere, but may also be enhanced by external disturbances, such as falling material.

*Subject headings:* sunspots — Sun: chromosphere — Sun: flares — Sun: photosphere — Sun: UV radiation

## 1. INTRODUCTION

Above sunspot light bridges, some dynamic activities, such as brightenings and surges, have been observed in the lower solar atmosphere (Asai et al. 2001; Shimizu et al. 2009; Louis et al. 2014; Tian et al. 2014; Toriumi et al. 2015a; Robustini et al. 2016). By examining the Doppler characters or the intensity variations in light bridges, a number of authors found evidence for the existence of oscillations in light bridges (Sobotka et al. 2013; Yuan et al. 2014; Yuan & Walsh 2016). With the high tempo-spatial resolution observations from the *Interface Region Imaging Spectrograph* (*IRIS*; De Pontieu et al. 2014), Yang et al. (2015) have found an ensemble of bright structures in the lower atmosphere rooted in a light bridge of NOAA Active Region (AR) 12192, and named this ensemble *light wall*. The most distinct character of the light wall is the existence of a much brighter wall top observed in *IRIS* 1330 Å images. The light wall showed evidence of oscillations in height, appearing as successive upward and downward motions of the wall top. This kind of oscillation, i.e., joint rising and falling motion of neighbouring bright structures, was also noted by Bharti (2015). We have interpreted that these oscillations of the light wall are due to the leakage of  $p$ -modes from below the photosphere (Yang et al. 2015). As the global resonant acoustic oscillations, the  $p$ -modes are deemed to leak sufficient energy to power shocks and thus drive upward flows (De Pontieu et al. 2004; Klim-

chuk 2006). Hou et al. (2016a) examined *IRIS* observations between 2014 December and 2015 June, and found that most light walls originate above light bridges.

In the present paper, we report our findings that the light wall can be significantly disturbed by external events, such as falling material. Due to the external disturbances, the wall base brightens and the wall height increases.

## 2. OBSERVATIONS AND DATA ANALYSIS

We use two series of slit-jaw images (SJIs) observed by *IRIS* on 2016 February 12 in 1330 Å. The 1330 Å pass-band includes a strong emission from the C II 1334/1335 Å lines which are formed in the chromosphere and lower transition region, and the continuum emission from the upper photosphere and lower chromosphere. The first series of SJIs were obtained from 17:23 UT to 18:34 UT and the second one from 22:15 UT to 23:25 UT. Both of the two series have a cadence of 10 s and a plate-scale of 0".166. Their field-of-view (FOV) is 119" × 119", covering the main sunspot of NOAA AR 12497. The two datasets have the same region (i.e., AR 12497) as target with solar-rotation tracking. The spectral data were obtained on the large coarse 4-step raster mode, and the slit crosses the path of the falling material.

During the two *IRIS* observational periods, we also obtained simultaneous intensity maps and magnetograms from the Helioseismic and Magnetic Imager (HMI; Scherrer et al. 2012; Schou et al. 2012) on-board the *Solar Dynamics Observatory* (*SDO*; Pesnell et al. 2012). The full-disk HMI data have a plate-scale of 0".5 and a cadence of 45 s. In addition, we use the 1600 Å images from the *SDO* Atmospheric Imaging Assembly (AIA; Lemen et al. 2012). The pixel size and cadence of the 1600 Å line are 0".6 and 24 s, respectively. Each sequence of

<sup>1</sup> Key Laboratory of Solar Activity, National Astronomical Observatories, Chinese Academy of Sciences, Beijing 100012, China; shuhongyang@nao.cas.cn

<sup>2</sup> College of Astronomy and Space Sciences, University of Chinese Academy of Sciences, Beijing 100049, China

<sup>3</sup> Solar Physics and Space Plasma Research Centre, School of Mathematics and Statistics, University of Sheffield, Hicks Building, Hounsfield Road, Sheffield S3 7RH, UK

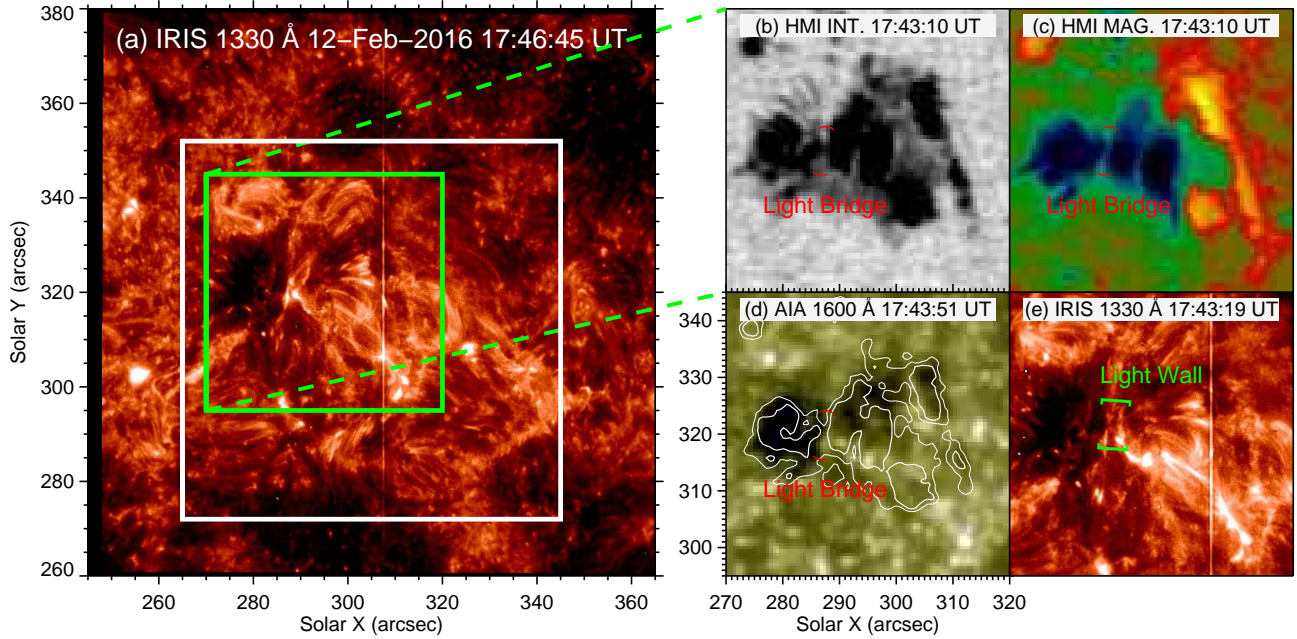


FIG. 1.— (a) *IRIS* SJI 1330 Å image observed on 2016 February 12. The green square outlines the FOV of Figures 1(b-e), and the white square outlines the FOV of Figure 2(a) and Figure 4. (b-e) HMI intensity map, HMI magnetogram, AIA 1600 Å image, and *IRIS* 1330 Å image showing the light bridge (marked by the red parentheses) and light wall (marked by the square brackets) within AR 12497. The white curves are the contours of sunspots identified in the HMI intensity map of panel (b).

the HMI and AIA data are calibrated to Level 1.5 with the standard procedure *aia\_prep.pro*, and differentially rotated to a reference time. The reference times for the two sequences are 17:46 UT and 22:38 UT, respectively.

### 3. RESULTS

An overview of AR 12497 in *IRIS* 1330 Å is shown in Figure 1(a). In the HMI intensity map (panel (b)) at 17:43 UT, there is a light bridge (outlined by the red parentheses) across the main sunspot. In the corresponding HMI magnetogram, the magnetic field at the light bridge is much weaker than the surrounding negative fields. The light bridge can be identified both in the AIA 1600 Å image (panel (d)) and *IRIS* 1330 Å image (panel (e)). Moreover, a light wall, i.e., an ensemble of bright structures rooted in the light bridge, is observed in the *IRIS* 1330 Å image, as denoted by the square brackets. The bright top of the light wall is somewhat conspicuous. The light wall cannot be identified in the AIA 1600 Å image.

#### 3.1. Disturbance by the falling material

In the south-west area near the light wall, a C6.8 flare occurred, as outlined by the blue circle in Figure 2(a). After that, a great deal of material was ejected into the corona (outlined by the blue dotted circle in Movie 1), and some of it descended downwards to the solar surface (denoted by the arrows in Movie 1). At 17:42:10 UT (see panel (b1)), the wall base and wall top are marked by the green dashed and dotted lines, respectively. Then, the falling material (indicated by the blue arrows in panels (b2) and (b3)) fell towards the base of the light wall. When the falling material reached the wall base at 17:44:28 UT, the landing point (outlined by the blue rectangle in panel (b3)) brightened. Meanwhile, more material as denoted by the green arrows in panel (b3) was

falling down. This material hit the wall base at 17:45:17 UT, and there was also a brightening at the landing point (outlined by the green circle in panel (b4)). Then, 39 s later, the brightening became more obvious (panel (b5)). Subsequently, the wall top began to rise (see panels (b5)-(b7)). At 17:46:45 UT, the wall top reached at a higher position (panel (b7)) compared to that of at 17:45:56 UT and 17:46:26 UT, respectively. Note that a large number of bright threads connecting the top and base of the light wall can be identified (marked by the blue dotted lines in panel (b7)), revealing the fanning out structure of the light wall. This can be used to explain why the wall with large increase in height is much larger than the brightened region at the wall base. Several minutes later, the top of the light wall began to fall back (see panel (b8)). We found that the bottom part of the light wall started to rise up prior to the main impact of the downflows. The reason may be that material was already falling prior to the main impact, which remains invisible at the *IRIS* resolution and temperature response.

To investigate the evolution of falling material and light wall, we make two time-distance diagrams along slices “A-B” and “C-D” (marked in Figure 2(b5)), respectively. The time-distance diagrams are presented in Figure 3. The base of the light wall is marked by the dashed line in each panel. The falling material appears as bright structures, and the leading and trailing edges are outlined by the two dotted lines in panel (a). When the falling material reaches the wall base with the projected velocity of  $71 \text{ km s}^{-1}$ , a range of brightenings appeared in the area outlined by the blue ellipse. The “+” symbol in panel (a) shows the first landing point of the falling material and the first brightening point around 17:45:30 UT. In panel (b), the green dotted curve outlines the variation of the bright wall top. When the first landing point became brightened (marked by the “+” symbol),

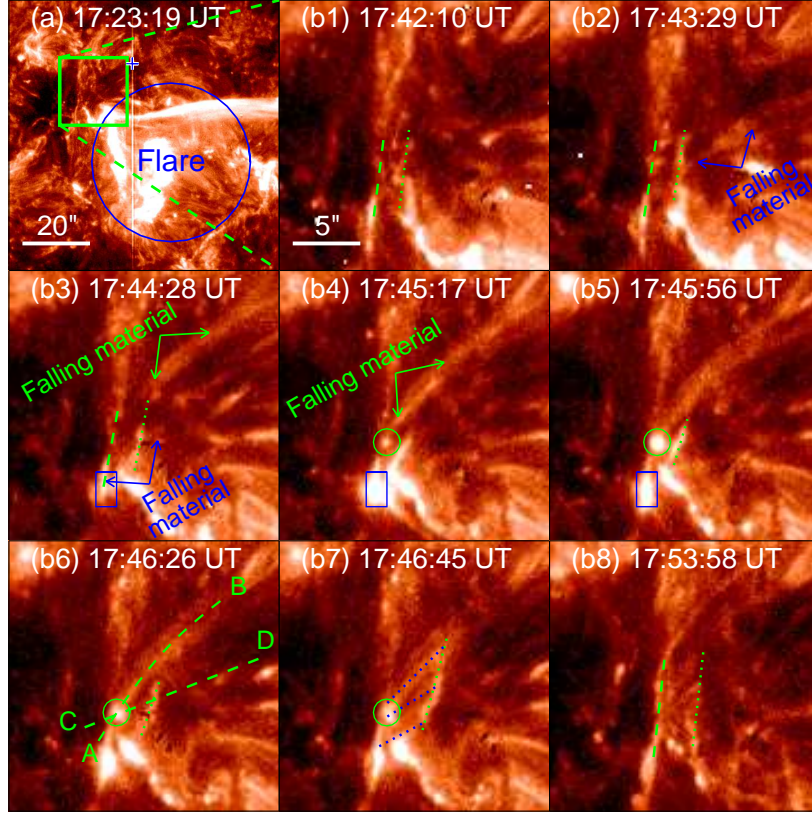


FIG. 2.— (a) *IRIS* 1330 Å image displaying the occurrence of a flare near the light wall (also see Movie 1). The square in panel (a) marks the FOV of panels (b1-b8), and the blue circle outlines the location where a flare occurred. The “+” symbol marks the position where the spectral profiles were analyzed. (b1-b8) Sequence of *IRIS* 1330 Å images showing the falling material (denoted by the arrows) and the evolution of the light wall. The green dashed and dotted lines indicate the positions of the wall base and wall top at different times. The blue rectangles and green circles outline the landing points of the falling material, also the brightening areas. The dashed curves “A-B” and “C-D” in panel (b6) mark the positions where the time-distance plots are obtained in Figure 3. The blue dotted lines in panel (b7) outline the bright threads connecting the top and base of the light wall.

the wall top rose quickly with an average velocity of  $60 \text{ km s}^{-1}$ . Due to the successive falling of material, several brightenings at the wall base appeared and the wall top moved upward (between the two blue dotted lines). The short streaks between the blue dotted lines are the characteristic of material due to the side motion of bright threads. The projected height of the light wall reached at the maximum of about 6.5 Mm at 17:50 UT, which is much higher than its height of 1.3 Mm just before the interaction with the falling material. Due to the projection effect, the real height of the light wall may be actually larger. Then, the height of the light wall began to decrease. At 17:54 UT, the projected height was 1.2 Mm, which is comparable to the one before the base brightenings. We analyzed the spectral profiles of Si IV 1393.78 Å in the path of the falling material (marked by the “+” symbol in Figure 2(a)). At 17:42:59 UT, the falling material was flowing across the slit, and by applying the Gaussian fitting method, we found that the red-shift relative to the background is about  $29 \text{ km s}^{-1}$ . Since the projected speed is  $71 \text{ km s}^{-1}$ , the total speed of the downflow is estimated to be  $77 \text{ km s}^{-1}$ .

### 3.2. Disturbance by the flare

In the larger FOV, outlined by the white window in Figure 1(a), next we study another flare and its effect on the light wall. At 22:17:57 UT, the base and top of the light wall can be well identified, and there was no observ-

able explosive event in the surrounding area (see Figure 4(a)). At 22:34:50 UT, the region outlined by the blue ellipse began to brighten (panel (b)), and then a C3.0 flare occurred (panel (c)). We note that, during the flare process, a bright channel which looks like a tail of the flare appeared, as indicated by the white arrow in panel (c). The bright channel extended from the flare towards the light wall. Then, the base of the light wall brightened and the height of the light wall increased. The bright channel was more evident at 22:38:16 UT (panel (d)). Although the flare decayed, the bright channel linking the flare and wall base remained clear for a while (panels (e)-(f)).

In order to study the response of the light wall during the flare, we display in Figures 5(a1)-(a6) a sequence of *IRIS* 1330 Å images in a small FOV (outlined by the green square in Figure 4(d)). In Figures 5(a1)-(a6), the dashed lines and dotted lines outline the wall base and wall top, respectively. Before the disturbance by the flare, the projected height of the light wall is about  $3.6''$  at 22:35:59 UT (panel (a1)). At 22:37:47 UT, the light wall was affected by the flare. Therefore the base of the light wall was brightened as denoted by the arrow in panel (a2), and the brightness of the wall top also increased, compared with that of 2 min earlier. Moreover, the wall top moved upwards quickly (panels (a2)-(a4)). A set of bright threads (outlined by the blue dotted lines in



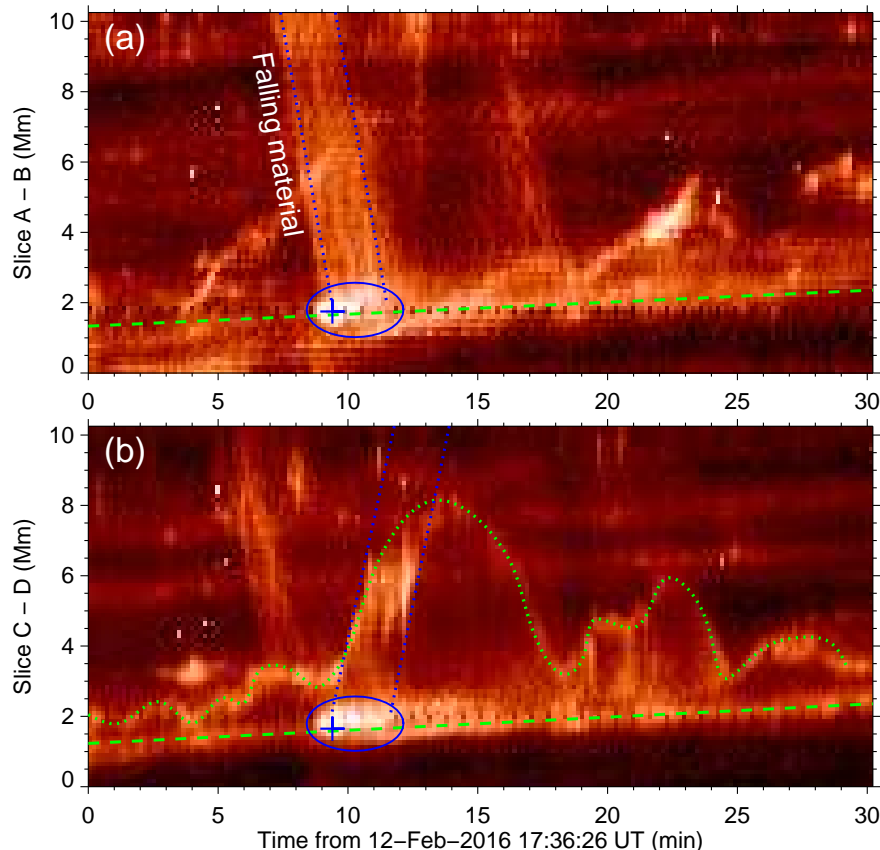


FIG. 3.— (a-b) Time-distance plots along slice “A-B” and “C-D” of Figure 2. The dashed lines mark the base of the light wall, and the green dotted curve delineates the wall top. The blue dotted lines in panel (a) outline the leading and trailing edges of the falling material, and those in panel (b) outline the upward motion of the wall top. The “+” symbols mark the first landing point of the falling material and brightening point. The ellipses outline the recurrent brightenings at the base of the light wall.

panel (b4)) connecting the wall base and wall top formed a fan-shaped structure. After that, the emission of the wall base decayed and the wall top moved downwards again (panels (a4)-(a6)), reaching at a lower height. In order to study the evolution of the light wall in more details, we make a time-distance plot along slice “A-B” marked in panel (a3), and present it in panel (b). In the time-distance plot, the green dashed line and dotted curve outline the wall base and wall top, respectively. We may see that, before 22:37 UT (marked by the left vertical line), the top of the light wall moved upward and downward with an average projected height of about 2.5 Mm. At 22:37 UT, the height of the light wall itself was about 2.5 Mm, as denoted by arrow “M”. Then, the wall base began to brighten at 22:37 UT, as marked by the blue “+” symbol. Subsequently, the height of the light wall increased quickly in the following 50 s (marked by the right vertical line) and became approximately 4.5 Mm (denoted by arrow “N”) in height. In the next 3 minutes, the wall base brightened continually and the wall top maintained its relatively high altitude. When the brightness of the wall base decreased, the top of the light wall fluctuated to lower heights. At last, the height of the light wall was comparable to that before the disturbance.

#### 4. CONCLUSIONS AND DISCUSSION

With *IRIS* observations, we study the dynamical evolution and response to external perturbations of a light

wall. A flare occurred near the light wall followed by material ejected into the corona from the lower solar atmosphere. Some of the ejected material fell back to the solar surface. When the falling material reached the light bridge, i.e., the base of the light wall, sudden brightenings appeared at the wall base and, most importantly, the wall top rose quickly, performing increase of the wall height. Once the brightenings of the wall base faded, the height of the light wall began to decrease. When another nearby flare took place, a bright channel was formed and extended from the flare towards the light bridge. Then, the wall base brightened and the height of the light wall began to increase again. Once again, when the brightness of the wall base decreased, the wall top fluctuated to lower heights.

Falling material slides down along magnetic field lines (Reale et al. 2013; Kleint et al. 2014; Innes et al. 2016; Jing et al. 2016). We suggest that the falling material shown in Figure 2 causes the brightenings of the wall base and the increase of the light wall height. The proposed scenario is as follows: When the falling material hits the light bridge, the kinetic energy is converted to the thermal energy. Due to the local associated heating, the light bridge brightens and the pressure of the plasma therein increases concurrently. The magnetic configuration of light wall is thought to be a group of magnetic field lines rooted in the light bridge (Hou et al. 2016b). Thus, the material is lifted at a much higher speed along magnetic field lines by the increased pressure at the bottom, lead-

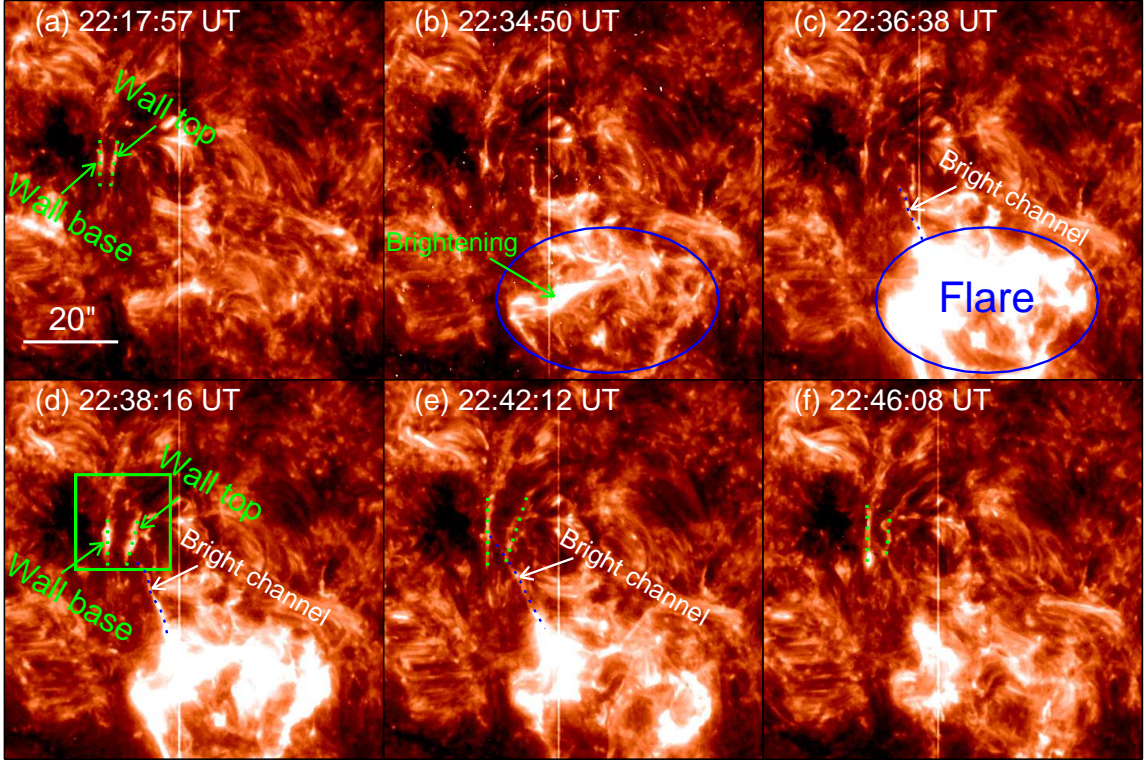


FIG. 4.— Sequence of *IRIS* 1330 Å images displaying the occurrence of another flare with a bright channel (blue dotted curves) connecting the light bridge (see also Movie 2). The blue ellipses outline the flare location.

ing to the observational phenomenon that the top of the light wall is powered to reach a greater height. A given magnetic flux loop often guides a large number of falling elongated blobs (Antolin et al. 2010; Antolin & Rouppe van der Voort 2012). Indeed, we can identify several blobs from the falling material (as shown in Movie 1), which appear as multi-trajectories marked between two dotted lines in Figure 3(a). The falling material continuously crashes into the wall base, leading to successive brightenings as outlined by the ellipses in Figures 3(a)-(b). Consequently, multi-trajectories of upward motion of the wall top are observed, as marked by two dotted curves in Figure 3(b).

Applying the methods of Gilbert et al. (2013) and Innes et al. (2016), the mass of falling material in Figure 3(a) is estimated to be about  $1.6 \times 10^{12}$  g. Since the total speed of the downflow is  $77 \text{ km s}^{-1}$ , then the kinetic energy is  $\sim 4.8 \times 10^{25}$  erg. This energy can power the light wall material to increase by 11 Mm in height. The observed height increase of the light wall shown in Figure 3(b) is consistent with this estimate. In addition, the rebound shock generated by the impact of falling material could indeed play some role in leading to the light wall's increase in height. Movie 1 and Figure 2 show that the falling material and the light wall are two separated structures in the corona, but they are joined at the foot-point (exactly very close to each other). Thus the impact of the falling material seems to affect a large region in the corona. This also implies that the falling material does not need to fall along the same path as the light wall to perturb it after the impact.

For the C3.0 flare, only a bright channel was observed. We suggest that, although no obvious material flow along

the bright channel was found, some amount of ejected material may still reach the light bridge. A somewhat similar process has been reported briefly by Yang et al. (2014). In that study, on three homologous confined flares, one remote region brightened when each flare occurred, which is also deemed to be caused by ejected material. For the present study, when the ejected particles along the bright channel impacted on the light bridge, kinetic energy is likely to be converted to thermal energy that heated the wall base and powered the light wall. For this case, we cannot fully exclude the possibility that the disturbance originates from below, such as small-scale reconnection in the lower atmosphere due to e.g. convection motion (Toriumi et al. 2015a, b). We note that there was a brightening at the wall base at 22:33 UT (indicated by the first arrow in Movie 2). This brightening only corresponds to a small increase of the wall height, much smaller than that resulted from the bright channel. Although it is difficult to determine the exact cause of the brightening at 22:33 UT, we think it may be caused by the small-scale reconnection due to the convection motion (Toriumi et al. 2015a, b).

We conjecture that a light wall is a slab-like structure (maybe even consisting of thin magnetic threads) embedded in vertically stratified plasma. Oscillations of light wall have earlier been interpreted to be powered by the leakage of  $p$ -modes from below the photosphere (Yang et al. 2015). Our new results reveal that the light wall can also be enhanced by external disturbances, such as falling material and an avalanche of particles caused by nearby flares.

We thank the referee for the helpful suggestions and

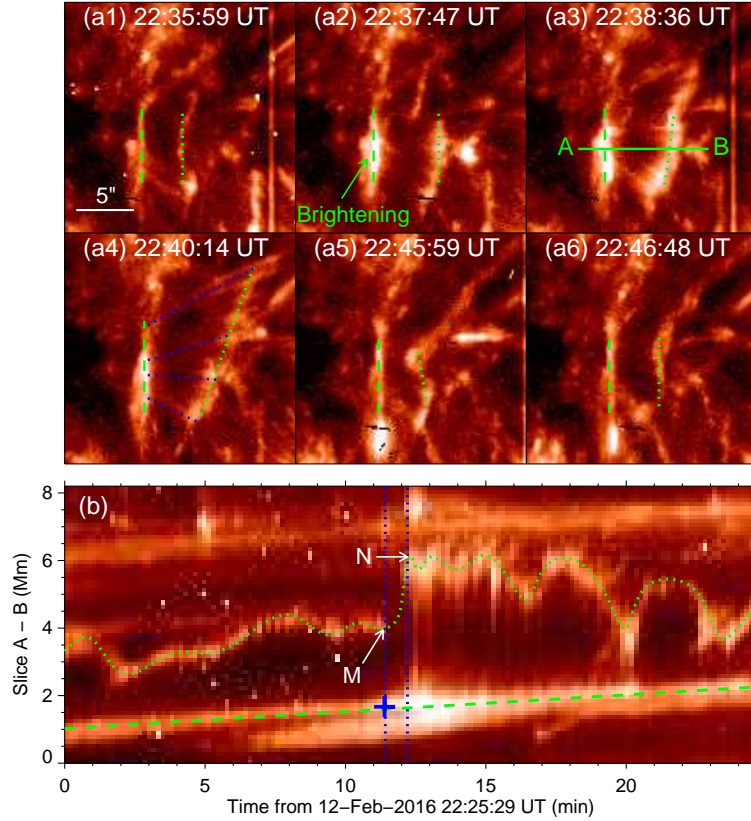


FIG. 5.— (a1-a6) *IRIS* 1330 Å images showing the evolution of the light wall impacted by the second flare. The green dashed and dotted lines mark the base and top of the light wall, respectively. The blue dotted lines in panel (a4) outline the fanning out bright threads connecting the top and base of the light wall. (b) Time-distance plot along slice “A-B” (marked in panel (a3)) derived from the 1330 Å images. The dashed line outlines the wall base and the dotted curve outlines the wall top, and the blue “+” symbol denotes the first brightening site. The left and right vertical lines mark the start and peak times of the disturbance, respectively. The arrows “M” and “N” denote the positions of the wall top at the start and peak disturbing times, respectively.

constructive comments. The data are used courtesy of *IRIS* and *SDO* science teams. This work is supported by the National Natural Science Foundations of China (11673035, 11533008, 11373004, 11303049, 11221063), the Strategic Priority Research Program (No. XDB09000000), the Youth Innovation Promotion Association of CAS (2014043), the CAS Project KJCX2-EW-

T07, and the Young Researcher Grant of National Astronomical Observatories of CAS. RE is grateful to STFC (UK) for the awarded Consolidated Grant, The Royal Society for the support received in a number of mobility grants. He also thanks the Chinese Academy of Sciences Presidents International Fellowship Initiative, Grant No. 2016VMA045 for support received.

#### REFERENCES

- Asai, A., Ishii, T. T., & Kurokawa, H. 2001, *ApJ*, 555, L65  
 Antolin, P., & Rouppe van der Voort, L. 2012, *ApJ*, 745, 152  
 Antolin, P., Shibata, K., & Vissers, G. 2010, *ApJ*, 716, 154  
 Bharti, L. 2015, *MNRAS*, 452, L16  
 De Pontieu, B., Erdélyi, R., & James, S. P. 2004, *Nature*, 430, 536  
 De Pontieu, B., Title, A. M., Lemen, J. R., et al. 2014, *Sol. Phys.*, 289, 2733  
 Gilbert, H. R., Inglis, A. R., Mays, M. L., et al. 2013, *ApJ*, 776, L12  
 Hou, Y. J., Li, T., Yang, S. H., & Zhang, J. 2016a, *A&A*, 589, L7  
 Hou, Y. J., Zhang, J., Li, T., Yang, S. H., et al. 2016b, *ApJ*, 829, L29  
 Innes, D. E., Heinrich, P., Inhester, B., & Guo, L. J. 2016, *A&A*, 592, A17  
 Jing, J., Xu, Y., Cao, W., et al. 2016, *Scientific Reports*, 6, 24319  
 Kleint, L., Antolin, P., Tian, H., et al. 2014, *ApJ*, 789, L42  
 Klimchuk, J. A. 2006, *Sol. Phys.*, 234, 41  
 Lemen, J. R., Title, A. M., Akin, D. J., et al. 2012, *Sol. Phys.*, 275, 17  
 Louis, R. E., Beck, C., & Ichimoto, K. 2014, *A&A*, 567, A96  
 Pesnell, W. D., Thompson, B. J., & Chamberlin, P. C. 2012, *Sol. Phys.*, 275, 3  
 Reale, F., Orlando, S., Testa, P., et al. 2013, *Science*, 341, 251  
 Robustini, C., Leenaarts, J., de la Cruz Rodriguez, J., & Rouppe van der Voort, L. 2016, *A&A*, 590, A57  
 Scherrer, P. H., Schou, J., Bush, R. I., et al. 2012, *Sol. Phys.*, 275, 207  
 Schou, J., Scherrer, P. H., Bush, R. I., et al. 2012, *Sol. Phys.*, 275, 229  
 Shimizu, T., Katsukawa, Y., Kubo, M., et al. 2009, *ApJ*, 696, L66  
 Sobotka, M., Švanda, M., Jurčák, J., et al. 2013, *A&A*, 560, A84  
 Tian, H., Kleint, L., Peter, H., et al. 2014, *ApJ*, 790, L29  
 Toriumi, S., Katsukawa, Y., & Cheung, M. C. M. 2015a, *ApJ*, 811, 137  
 Toriumi, S., Cheung, M. C. M., & Katsukawa, Y. 2015b, *ApJ*, 811, 138  
 Yang, S. H., Zhang, J., & Xiang, Y. Y. 2014, *ApJ*, 793, L28  
 Yang, S. H., Zhang, J., Jiang, F. Y., & Xiang, Y. Y. 2015, *ApJ*, 804, L27  
 Yuan, D., Nakariakov, V. M., Huang, Z., et al. 2014, *ApJ*, 792, 41  
 Yuan, D., & Walsh, R. W. 2016, *A&A*, 594, A101